Paper

On the Energy Distribution of Secondary Electrons Emitted from Metals

Z. J. Ding,[a,*] H.M. Li,[b] R. Shimizu,[c] and K. Goto[d]
[a]*Hefei National Laboratory for Physical Sciences at Microscale and Department of Physics, University of Science and Technology of China, Hefei 230026, Anhui, People's Republic of China*
[b]*USTC-HP Labortary of High Performance Computing, University of Science and Technology of China, Hefei 230026, Anhui, People's Republic of China*
[c]*International Institute for Advanced Studies, 9-3 Kizugawa-dai, Kizugawa-City, Kyoto 619-0225, Japan*
[d]*National Institute of Advanced Industrial Science and Technology (AIST) Chubu, Moriyama-ku, Nagoya, Aichi 463-8560, Japan*
[*]*zjding@ustc.edu.cn*

(Received: March 25, 2008; Accepted: May 10, 2008)

The energy distribution of secondary electrons emitted from several metals has been investigated theoretically and a comparison of Monte Carlo simulation result with an experimental measurement has been made. The Monte Carlo simulation of cascade secondary electron production is based on the use of a dielectric function for the treatment of electron inelastic scattering and secondary excitation, and on the use of Mott cross section for describing electron elastic scattering. The calculation reproduces well the weak features presented in the experimental energy spectra of secondary electrons measured with a cylindrical mirror analyzer. The result indicates that, the weak feature is resulted from the directly emitted secondary electrons after generation without energy loss processes and, thus, carries the characteristic energy transferred from the loss energy of the incident electrons. However, during their transportation to the surface much of the cascade secondary electrons have suffered quite energy losses and to be presented as the large background.

1. Introduction

Electron scattering process near a sample surface forms the physical basis in surface characterization techniques by using electron microscopy and electron spectroscopy. In particular, the phenomena of electron backscattering and secondary electron emission from solids bombarded by a primary electron beam are basic to scanning electron microscopy [1] and Auger electron spectroscopy. Many experimental measurements on secondary electron emission have been done since 1960's and these observations have revealed following common facts about secondary electrons emission from metal surfaces [2-6]: 1. The energy spectra of secondary electrons are peaked at about 1-5 eV above the vacuum level; with increasing energy from the vacuum level the spectra shape shows a quick raising to the peak and then a slower reduction of the intensity. The full width of the peak is around 3-15 eV. The energy distribution curve is thus quite universal for metals, when normalized at their most probable energies; 2. As at energy of several tens eV the intensity of energy spectra is much weakened as compared with the maximum peak height for enough high primary energies, therefore, a convenient definition of the true secondary electrons is such that their energies are less than 50 eV, and, the backscattering electrons are defined as that their energies are greater than 50 eV. For the yield of secondary electrons, i.e. the area under the energy distribution curve which is measured with a retarding field energy analyzer for true secondary electrons emitted into the whole hemi-spherical solid angles about the sample surface and is normalized with the primary beam current, it shows a universal primary energy dependence while the maximum yield and the corresponding primary energy are material dependant parameters.

Also, the values of secondary electron yield can be even larger than the unit.

These characters of secondary emission, hence, implies the mechanism of secondary electron generation through a cascade process because only in this way the amount of secondary electrons generated inside the sample can be multiplied so that the emitted current may even be higher than the incident current. The chief feature of the energy distribution of secondary electrons can also be understood: the cascade process produces much of low energy electrons inside the sample and the energy distribution is then monotonously increasing with decreasing energy; therefore, by also considering the angular distribution of secondary electron emission from the surface when overcoming the surface barrier the energy distribution exhibits a peak at an energy above the surface barrier.

However, despite the universal shape of secondary electron spectra many experiments have show that there are some quite weak features presented in the energy distribution for clean surfaces. Several mechanisms had been considered for the creation of these fine structures [7], i.e. diffraction phenomena for single crystal surfaces [8], plasmon decay [9-10], interband transitions [11-12], Auger transitions etc. The electron energy loss spectroscopy has been used to correlate the energy loss peaks with features in secondary electron spectra in order to indentify the mechanisms via plasmon decay for free electron-like metals and/or interband transition for noble and transition metals.

Theories about secondary electron emission have been developed accordingly [13]. A simple treatment considers electron excitation based on the Sommerfeld free electron model [14]. Later on the concept about secondary electron cascade process describing the diffusion, energy loss, and multiplication within a metal is suggested with the use of transport equation method [15]. These earlier analytical theories cannot certainly account for the respective details of electron excitation and emission in each metal. Since the propose of plasmon decay pathway [9], efforts have been put forward mainly on the typical free electron-like metal, Al. Calculation of energy distribution and secondary electron yield has been carried out with both Monte Carlo method [10] and transport equation [9,13], based on the framework of Lindhard dielectric function formulation to describe free electron excitation and the electron excitation via plasmon decay. However, it should be noted that two experimental measurements for Si [16] and Al [17] by coincidence electron spectroscopy seems controversial on the role of plasmon decay in secondary electron production.

Monte Carlo simulation method has been playing the most important role in the calculation of various physical parameters related to secondary emission. A full description of the secondary emission phenomena consists of three elementary processes: generation, transport and emission. Several typical algorithms used for the modelling of secondary electron excitation are: by using a single particle excitation function [18] with simple cascade transport [19], a straightforward assignment of secondary excitation with cascade transport [20,21], a direct estimation of emission yield from stopping power equation and emission probability with parameters [22], using the Lindhard dielectric function formulation for Al with cascade process [10]. These studies are either not based on a detailed microscopic model of secondary electron excitation so that not to be specific to a material, or, only limited to free electron-like metal. Therefore, they are hardly applied to the study of particular energy distribution for other ones than free electron-like metals. In this respect a model of secondary electron excitation based on a dielectric function formulation but by using experimental optical data [23,24] may provide a useful insight about the features of secondary electron emission that are characteristic to a specific metal. The detailed theoretical understanding of secondary electron emission problem requires, hence, a systematic Monte Carlo investigation over many materials; furthermore, it is necessary for a Monte Carlo modeling to handle both the energy distribution curve and the yield data in order to obtain a full understanding of the problem.

In our previous works we have investigated backscattering electron energy spectra with cascade secondary electrons included [25,26]; the relative intensity calculated agrees excellently well with the experimental $N(E)$ curve of backscattering background of Auger electron spectroscopy spectra that measured by Goto and coworkers with their novel cylindrical mirror analyzer (CMA) [27,28]. It is further shown that both the simulated absolute secondary electron yields for several metals and the relative yield curve for about twenty metals

[29,30] are in reasonable agreement with the available experimental data. In this work we will study the features presented in the energy distribution of secondary electrons for several transition and noble metals. The calculated secondary electron spectra are obtained simultaneously with the backscattering continuum, the low loss features and the elastic peak from the vacuum level up to primary energy of incident electrons. The comparison will be made with the experimental $N(E)$ curve of secondary electrons measured also by the CMA.

2. Theoretical

In order to model the feature of secondary electrons, it is necessary to take electronic structure into consideration [31]. Here we shall consider a simple algorithm to include the band structure effect by using directly optical energy loss function of metals. The main idea is that the effect of interband transition that may contribute to secondary electron excitation is most appropriately modeled by the experimental data of optical energy loss function, which are used in the calculation of electron inelastic scattering mean free path and energy loss distribution. Our Monte Carlo model of electron-solid interaction for the simulation of secondary electron generation [23,25-28] is based on the use of Mott cross section in describing electron elastic scattering and a dielectric approach to electron inelastic scattering. Here we shall present only the outline of the simulation model.

The relativistic expression of electron-atom scattering, the Mott differential cross section, is given by

$$\frac{\mathrm{d}\sigma_e}{\mathrm{d}\Omega} = \left|f(\theta)\right|^2 + \left|g(\theta)\right|^2 \tag{1}$$

with the scattering amplitudes

$$f(\theta) = \frac{1}{2ik}\sum_{\ell=0}^{\infty}\left\{(\ell+1)\left(e^{i2\delta_\ell^+}-1\right)+\ell\left(e^{i2\delta_\ell^-}-1\right)\right\}P_\ell(\cos\theta); \tag{2}$$

$$g(\theta) = \frac{1}{2ik}\sum_{\ell=1}^{\infty}\left\{-e^{i2\delta_\ell^+}+e^{i2\delta_\ell^-}\right\}P_\ell^1(\cos\theta),$$

where $P_\ell(\cos\theta)$ and $P_\ell^1(\cos\theta)$ are, respectively, Legendre and the first order associated Legendre functions. δ_ℓ^+ and δ_ℓ^- are spin *up* and spin *down* phase shifts of ℓ th partial wave, respectively. Phase shifts are numerically evaluated by solving the Dirac equation for the radial part of the wave function of the scattering electron in an atomic potential field for Thomas-Fermi-Dirac atom.

The differential cross section for electron inelastic scattering in a solid is represented in dielectric theory in terms of the energy loss function, $\mathrm{Im}\{-1/\varepsilon(\mathbf{q},\omega)\}$, as

$$\frac{d^2\lambda_{in}^{-1}}{d(\hbar\omega)dq} = \frac{1}{\pi a_0 E}\mathrm{Im}\left\{\frac{-1}{\varepsilon(q,\omega)}\right\}\frac{1}{q} \tag{3}$$

where $\hbar\omega$ and $\hbar q$ are the energy loss and the momentum transfer, respectively, from an electron of kinetic energy E penetrating into a solid of dielectric function, $\varepsilon(\mathbf{q},\omega)$. λ_{in} is the electron inelastic mean free path. The wave vector- and frequency-dependent energy loss function may be derived from optical dielectric data $\varepsilon(\omega)$. The method extends the optical energy loss function, $\mathrm{Im}\{-1/\varepsilon(\omega)\}$, to the corresponding $\mathrm{Im}\{-1/\varepsilon(\mathbf{q},\omega)\}$ at finite q-values along the plasmon-pole dispersion curve [23]. This modeling of electron energy loss processes includes plasmon excitation, interband transition and inner-shell ionization.

The double differential inelastic mean free path respect to loss energy $\Delta E=\hbar\omega$ and scattering solid angle is given by

$$\frac{d^2\lambda_{in}^{-1}}{d(\Delta E)d\Omega} = \frac{1}{(\pi a_0 e)^2 E}\mathrm{Im}\left\{\frac{-1}{\varepsilon(q,\omega)}\right\}\frac{1}{q^2}\sqrt{E(E-\Delta E)}. \tag{4}$$

From above equation we can determine the specific energy loss and the corresponding angle of deflection in a particular inelastic scattering event in tracing an electron trajectory. The compiled optical data [32] for metals were used in the simulation.

We assume that each individual inelastic collision may produce a knock-on secondary electron by transferring the loss energy ΔE to an inner-shell electron or a valence-conduction electron. The scattered electron of initial energy E thus has energy $E-\Delta E$ after an inelastic collision. Then, an excited secondary electron has energy $E_s=\Delta E-E_B$ if it is generated from an inner-shell ionization ($\hbar\omega_0>E_B$), where E_B is the binding energy of the outermost inner-shell edge clearly present in an optical energy loss function and $\hbar\omega_0$ is the ionization energy derived from ΔE by the dispersion equation. Otherwise, it is an excitation of one electron of energy E' above the bottom of the conduction band with the probability distribution, $P(E',\Delta E)\propto[E'(E'+\Delta E)]^{1/2}$, which is assumed to be proportional to the density of states for a free electron gas [13]. The excited secondary electron then gains the energy $E_s=E'+\Delta E$. In this respect, our approach is different from the previous model [23] in which the probability for secondary-electron production was assumed to be

unity.

Secondary electrons follow the similar scattering processes as the primary electrons. The inelastic scattering process proceeds with the successive production of secondaries, and leads to the generation of a large number of secondary electrons at low energies. This cascade multiplicative process of secondary population is tracked in the simulation until all secondary electrons either escape from the surface or come to rest within the sample. In the simulation we can distinguish the diffused primary electrons and cascade secondary electrons as follows: Among the trajectories for each primary electron incident on the target, only one trajectory that successively loses energy from the primary energy and has the energy $E-\Delta E$ after an inelastic scattering event is considered as the diffused primary electron; all other electrons are regarded as cascade secondaries. A quantum transmission function is applied to electron emission from the surface as it is necessary to consider refraction of electrons by the potential barrier at the surface [33]. We have neglected the creation, emission and scattering of Auger electrons in the simulation.

3. Experimental

A CMA system [27,28] was used to measure the energy spectra of backscattered electrons and secondary electrons at normal incidence condition. This CMA, equipped with a coaxial electron gun, detects electrons with a Faraday cup (>99% efficiency) connected to an electrometer to allow absolute measurement of the signal-electron current for a particular primary-beam current. The emitted electrons enter the CMA at the usual angle of 42.3°±6° and the energy resolution is 0.24%. Special care has been paid to reduce the fringing effect of electric fields (<0.1%) as well as to shield the magnetic field (<1mG). The interior of the CMA as well as almost all parts that electrons can hit were coated with aquadag and soot to reduce scattering of electrons in the CMA. The spectral background due to internally scattered electrons was estimated to be less than 0.1-0.2% of the energy distribution. A precision high-voltage divider inserted between the output of the power supply and the CMA was used to measure voltages up to 5 kV with an accuracy of 0.1 V.

The CMA system was evacuated into the 10^{-9} Pa range and experiments were performed in the low 10^{-8} Pa range. The pure polycrystalline metal samples, unless specified otherwise, were mechanically polished to a mirror surface, and then briefly bombarded by 200-500 eV argon ions. Once cleaned, the sample surfaces could remain clean for several months. The spectra were recorded with stable primary currents (±1%) of 1.00 μA and 100 nA for accelerating voltages of 1-5 kV and below 1 kV, respectively, and the latter spectra were scaled to those with primary currents of 1 μA.

4. Results and discussion

Figure1 shows the measured energy distributions of secondary electrons emitted from several metals varied primary energies. This $N(E)$ distribution is obtained from the directly measured $EN(E)$ spectrum by dividing the intensity with energy E. The secondary electron peaks are found to be located at 5-10 eV, which are about several eV more than those measured with a retarding field energy analyzer. This may be due to the effect of fringing electric field and residual magnetic field in the CMA on the very slow (<5 eV) electrons. By varying primary energy the spectra intensity changes, however, the dominant features remain at the same energy position. One can find that, for Ta and W, there is a weak hump presented in the descending slope at the higher energy side of the peak. The position of feature is independent of the primary energy. However, for Au and Cu, the descending slope is rather smooth without an obvious feature.

The Monte Carlo calculations were performed for primary beam of energies from 100 eV to 5000 eV at normal incidence. Only those results for several metals at primary energy of 500 eV will be presented here as the comparison with experiment is very similar at other primary energies. In each case we have traced primary electron trajectories as many as 5×10^7 and about ten times more the secondary electron trajectories inside the sample.

Figure 2 shows the comparison on the energy distribution of secondary electrons between the Monte Carlo simulation result and the experimental measurement with a CMA for Ta and W. In the presented simulation spectra we have counted all the emitted secondary electrons, i.e. the solid angles for detection are whole hemisphere, without considering the solid angles for detection by CMA. This is because we need only to consider the rela-

tive intensity curve here and the energy spectra is, in fact, independent of the angular distribution for secondary electrons. It is clear that the simulation reproduces well the features observed in the experimental spectra. For Ta,

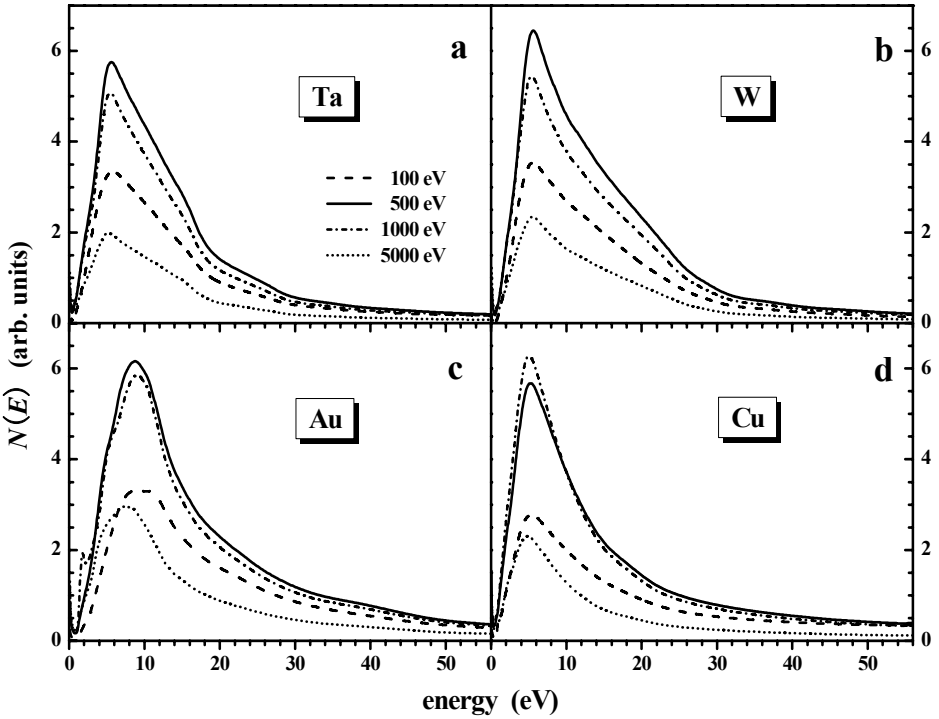

Fig. 1. Measured energy spectra of secondary electrons at primary energies of 100, 500, 1000 and 5000 eV for metals: (a) Ta; (b) W; (c) Au; (d) Cu.

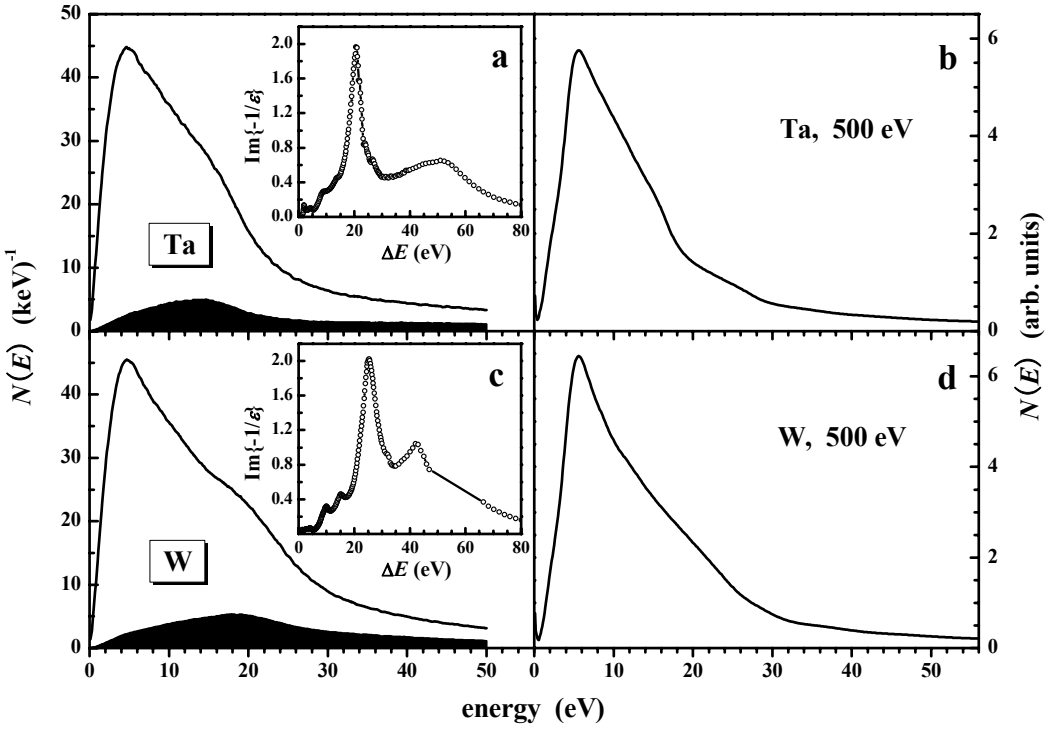

Fig. 2. Comparison between the simulated and the measured energy spectra of secondary electrons at primary energy of 500 eV for Ta and W. The inset figure shows the energy loss function of the respective metal. (a) Ta (calculation); (b) Ta (experiment); (c) W (calculation); (d) W (experiment).

there is a hump at 14-16 eV for both experimental and theoretical spectra. For W, the hump at 18-20 eV is somewhat stronger than that observed in the experimental spectra; however, the general feature of the spectra shape is rather similar.

To identify the origin of the feature we illustrate the spectra for directly emitted secondary electrons in the figure by the shade area. These secondary electrons are elastically transported to the surface for emission without suffering any energy loss since their generation beneath the surface. It is clear that they are responsible for the feature presented in the energy spectra. Other cascade electrons having undergone inelastic processes then form the large smooth background. In the inset figure we show the optical energy loss function $\mathrm{Im}\{-1/\varepsilon(\omega)\}$ that used in the simulation. By the present simulation model, a secondary electron is excited by receiving an energy loss from an inelastic scattering electron, i.e. $E_S=E'+\Delta E$, where E' is taken from 0 up to Fermi energy E_F. When it is elastically emitted from the surface, its kinetic energy measured from the vacuum level will be subtracted by an inner potential $U=E_F+\phi$, where ϕ is the work function. For Ta, ϕ = 4.1 eV and $\mathrm{Im}\{-1/\varepsilon(\omega)\}$ has a peak at 20.6 eV so that the maximum probability of loss energy is occurred for $\Delta E\approx$20 eV. It is this peak in the energy loss function results in the weak hump at about 16 eV in the energy spectra of secondary electrons. Likewise, for W, ϕ = 4.6 eV and $\mathrm{Im}\{-1/\varepsilon(\omega)\}$ has a peak at 25 eV so that the hump appears around 20 eV. Therefore, such observation explains reasonably the single electron excitation behavior in these refractory metals.

In contrast, for some noble and transition metals like Au and Cu, their energy loss function does not exhibit a sharp singular peak at lower loss energies of several tens of eV. Therefore, as shown by Fig.3, both the experimental and theoretical spectra display the smooth slope for the spectra shape without an obvious hump. This is because the spectra for directly emitted secondary electrons shown by the shade area are also very flat. From the energy loss function of these metals we can find that the function has a rather broad distribution around several tens eV; the small peaks located at 16 and 26 eV for Au and at 10, 19 and 28 eV for Cu can therefore not be shown its effect on the energy distribution of secondary electrons. Similar behavior can also be found for Ag. As shown by Fig.4(a), the energy loss function of silver has a strong sharp peak at 3.8 eV due to bulk plasmon excitation, which can not present a feature in the energy distribution of secondary electrons because its too narrow plasmon peak contributes actually a small value to oscillator strength; while other peaks are superimposed on a broad distribution extending from 0 to 100 eV like the

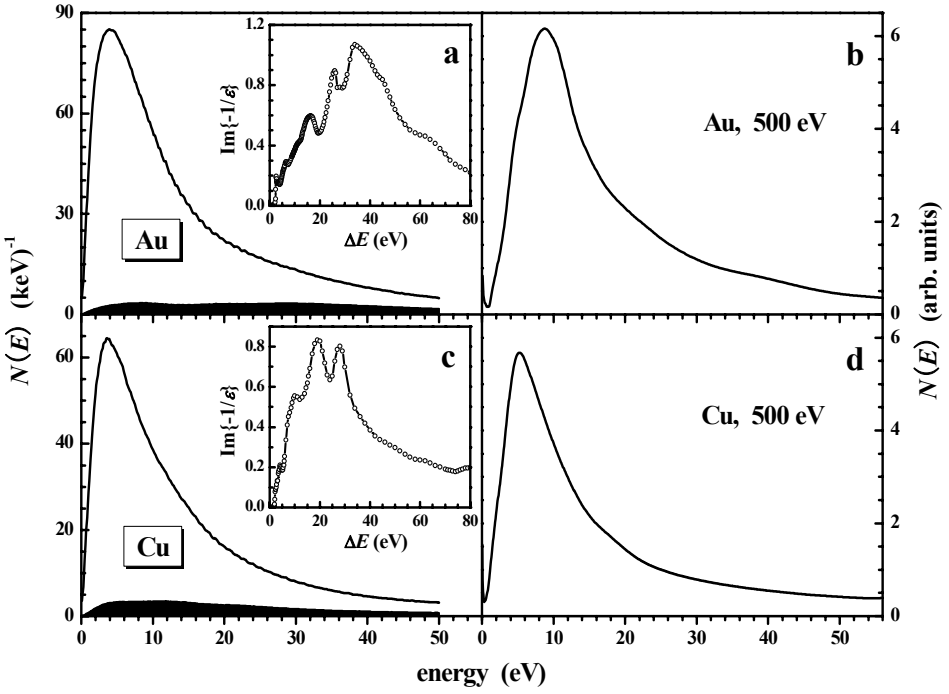

Fig. 3. Comparison between the simulated and the measured energy spectra of secondary electrons at primary energy of 500 eV for Au and Cu. The inset figure shows the energy loss function of the respective metal. (a) Au (calculation); (b) Au (experiment); (c) Cu (calculation); (d) Cu (experiment).

case of Au. Therefore, the slope of the experimental spectra shape is quite smooth although there is a slight difference on the spectra shape around the peak region between the experiment and calculation.

Even though in many cases the agreement on the energy spectra shape between the experimental measurement and the simulation result is very satisfactory, however, the case of noble metal Pt shows a larger deviation. Because the energy loss function of Pt has a moderate broaden peak at 33 eV, there is a very weak hump around 26-28 eV in the simulated energy spectra shown by Fig.4(c). But the experimental spectra display a faint concave shape in the corresponding energy region (Fig.4 (d)). From the theoretical aspect there are several approximations employed in the present calculation that may lead to such a derivation for specific materials: the single electron excitation mechanism by considering a simple probability distribution, $P(E',\Delta E)\propto[E'(E'+\Delta E)]^{1/2}$, for the density of states of a free electron gas; the derivation of the general energy loss function, $\mathrm{Im}\{-1/\varepsilon(\mathbf{q},\omega)\}$, with the use of optical energy loss function, $\mathrm{Im}\{-1/\varepsilon(\omega)\}$, in the plasmon pole approximation. It is quite possible that the density of states for the valence band influences not only the energy loss distribution but also the excitation function.

Figure 5 shows other calculated energy spectra of secondary electrons for metals, Nb, V, Ir and Rh. All these metals display strong peaks in the loss energy range 10-50 eV, and, there are corresponding features presented in the secondary electron spectra. These calculated spectra need to be verified by further experimental measurement.

It should be mentioned that, however, the present theoretical approach cannot be applied to the free electron-like materials including Al, Be, C and Si for which a strong bulk plasmon peak at $\hbar\omega_p$ dominates the energy loss function. According to the present simulation model a strong false peak would appear at $\hbar\omega_p-\phi$, in addition to the usual maximum peak at 3-5 eV, by using such an optical energy loss function and single pole approximation. The experimental spectra for Al show that, like other metals, there is only a weak hump at$\hbar\omega_p-\phi$. The reason for the failing of the theoretical modeling for these materials is attributed to two facts: Firstly, the plasmon pole approximation is of problem to derive excitation function of secondary electron generation via the optical data. The more accurate Lindhard dielectric function illustrates that, for free electron-like metal like Al, in addition to a bulk plasmon dispersion curve which will be terminated at certain wave-vector length, there is a

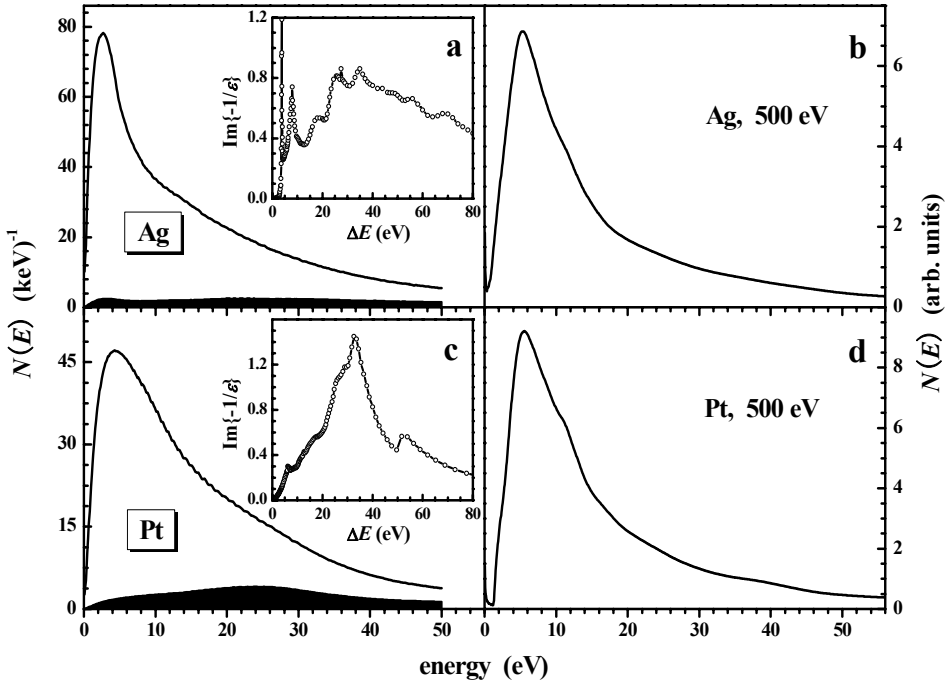

Fig. 4. Comparison between the simulated and the measured energy spectra of secondary electrons at primary energy of 500 eV for Ag and Pt. The inset figure shows the energy loss function of the respective metal. (a) Ag (calculation); (b) Ag (experiment); (c) Pt (calculation); (d) Pt (experiment).

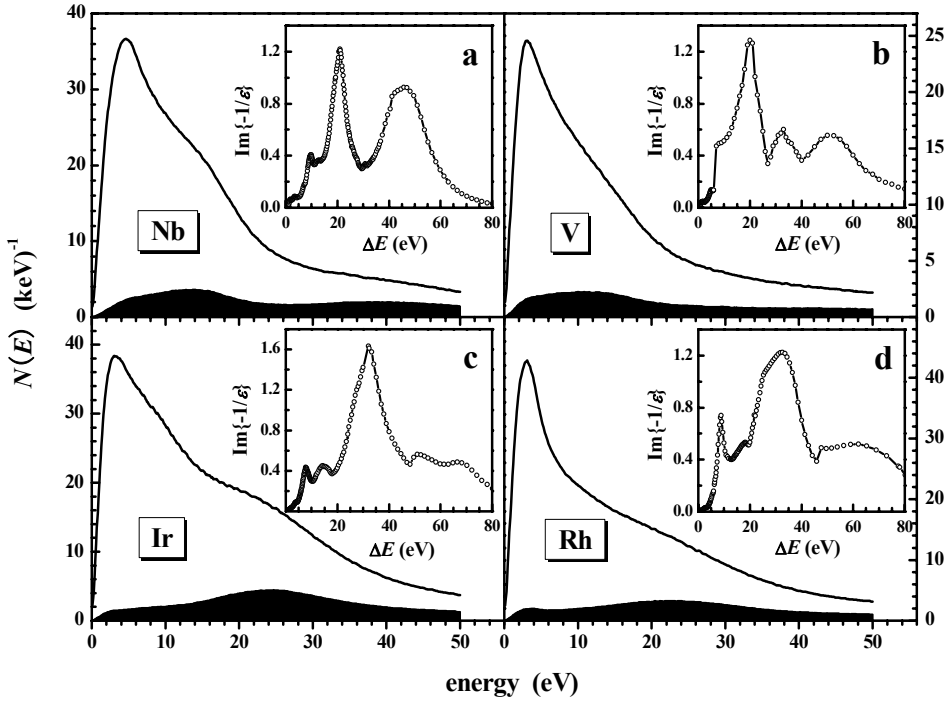

Fig. 5. The simulated energy spectra of secondary electrons at primary energy of 500 eV for (a) Nb; (b) V; (c) Ir; (d) Rh. The inset figure shows the energy loss function of the respective metal.

single particle excitation area in (ω,q). Therefore, the excited secondary electron should be broadly distributed in energy via single electron excitation. But, by the present plasmon pole approximation the energy loss function extends a single plasmon peak to infinite wave-vector length and, in fact, the single electron excitation is neglected. The approximation is reasonable for noble and transition metals that do not exhibit a single strong bulk plasmon peak in optical energy loss function. Secondly, as the loss energy is assumed to be transferred to an excited secondary electron, any energy loss at $\hbar\omega_p$ in fact implies a single electron excitation via plasmon damping mechanism. However, such a mechanism has not been verified. Previous studies had assumed multiple particle excitations to share the energy $\hbar\omega_p$ for a plasmon damping event [10]. The characteristic energy can be smeared out by such a mechanism. Therefore, special consideration should be paid for these materials in another study undertaken [34] and it is difficult to include every case in the present general simulation algorithm.

5. Conclusions

Based on a Monte Carlo simulation model of electron interaction with solids including cascade secondary electron production, we have investigated secondary electron generation and emission for several metals. Particular attention is paid on the weak features presented in the energy distribution. The electronic structure effect is modeled with an optical dielectric function for describing electron energy loss and the associated secondary electron excitation. The simulated energy distributions have been well compared with the experimental energy spectra measured with a CMA. For Ta and W, some weak features are found around 14-16 and 18-20 eV, respectively. The simulation result has indentified that they are attributed to the directly emitted secondary electrons after generation, which are elastically transported to the surface for emission without suffering any energy loss. These electrons carry the characteristic energy transferred from the loss energy of the incident electrons, while cascade secondary electron production would produce the usual large background for the secondary energy distribution curve. Thus, for a metal whose optical energy loss function Im{-1/$\varepsilon(\omega)$} has a rather intensive sharp peak, there would be a corresponding hump in the energy distribution. For other metals like Au and Cu, whose energy loss function does not exhibit such a sharp singular peak at lower loss energies of several tens of eV, both the experimental and theoretical spectra display the smooth slope for the spectra shape without an obvious

hump. The more accurate calculation of the energy distribution curve can be carried out with a density of states other than that of a free electron-like metal that employed in this calculation.

6. Acknowledgements

This work was supported by the National Natural Science Foundation of China (Grant Nos. 10025420, 10574121, 10874160), "111 Project", Chinese Education Ministry and Chinese Academy of Sciences.

7. References

[1] L. Reimer, *Scanning Electron Microscopy*, 2nd Ed. (Springer-Verlag, New York, 1998).

[2] A. J. Dekker, *Solid State Phys*. **6**, ed. F. Seitz and D. Turnbull (Academic, New York, 1958) p. 232.

[3] C. Hachenburg, W. Bauer, *Adv. Electr. Electron Phys*. **11**, 413 (1959).

[4] H. Seiler, *J. Appl. Phys*. **54**, R1 (1983).

[5] R. Kollath, In: *Encyclopedia of Physics*, vol. **21**, ed. S. Flugge (Springer, Berlin, 1956) p.232.

[6] J. Schafer and J. Holzl, *Thin Solid Films* **18**, 81(1972).

[7] M. Cailler and J. P. Ganachaud, *Scanning Microsc. Suppl*. **4**,57 (1990).

[8] K. Goto and K. Ishikawa, *J. Appl. Phys*. **43**, 1559 (1972).

[9] M. S. Chung and T. E. Everhart, *Phys. Rev. B* **15**, 4699 (1977).

[10] J. P. Ganachaud and M. Cailler, *Surf. Sci*. **83**, 498 (1979); **83**,519 (1979).

[11] M. Cailler, J. Pillon, D. Roptin, J. P. Ganachaud, H. Mignot, and C. Dejardin-Horgues, Rapport ATP CNRS, 1977.

[12] O. F. Panchenko and L. K. Panchenkoa, *Vacuum* **81**, 766 (2007).

[13] A. Dubus, J. C. Dehaes, J. P. Ganachaud, A. Hafni, and M. Cailler, *Phys. Rev. B* **47**, 11056 (1993).

[14] E. M. Baroody, *Phys. Rev*. **78**, 780 (1950).

[15] P. A. Wolff, *Phys. Rev*. **95**, 56 (1954).

[16] M. R. Scheinfein, J. Drucker, and J. K. Weiss, J. Microsc. **47**, 4068 (1993).

[17] W. S. M. Werner, G. Stefani, A. Ruocco, S. Lacobucci, F. Offi, and W. Smekal, ECASIA-07, QUA-1618.

[18] H. W. Streitwolf, *Ann. Phys*. **458**, 153 (1959).

[19] T. Koshikawa and R. Shimizu, *J. Phys. D: Appl. Phys*. **7**, 1303 (1974).

[20] S. Luo and D. C. Joy, *Scanning Microsc. Suppl*. **4**, 127 (1990).

[21] T. E. Allen, R. R. Kunz, and T. M. Mayer, *J. Vac. Sci. Technol. B* **6**, 2057 (1988).

[22] Y. Lin and D.C. Joy, *Surf. Interface Anal.* **37**, 895 (2005).

[23] Z. J. Ding and R. Shimizu, *Scanning* **18**, 92 (1996).

[24] J.-Ch. Kuhr and H.-J. Fitting, *J. Elect. Spectrosc. Rela. Phenom.* **105**, 257 (1999).

[25] Z. J. Ding, T. Nagatomi, R. Shimizu, and K. Goto, *Surf. Sci.* **336**, 397 (1995).

[26] Z. J. Ding, H. M. Li, K. Goto, Y. Z. Jiang, and R. Shimizu, *J. Appl. Phys*. **96**, 4598 (2004).

[27] K. Goto, N. Sakakibara, Y. Takeichi, Y. Numata, and Y. Sakai, *Surf. Interface Anal.* **22**, 75 (1994).

[28] Y. Takeichi and K. Goto, *Surf. Interface Anal.* **25**, 17 (1997).

[29] Z. J. Ding, X. D. Tang, and R. Shimizu, *J. Appl. Phys*. **89**, 718 (2001).

[30] Z. J. Ding, H. M. Li, X. D. Tang, and R. Shimizu, *Appl. Phys. A* **78**, 585 (2004).

[31] N. E. Christensen and R. F. Willis, *J. Phys. C: Solid State Phys*. **12**, 167 (1979).

[32] E. D. Palik (ed.), *Handbook of Optical Constants of Solids* (Academic, Orlando, 1985).

[33] R. Shimizu and Z. J. Ding, *Rep. Prog. Phys.* **55,** 487 (1992).

[34] S.F. Mao, Y.G. Li, R.G. Zeng and Z.J. Ding, J. Appl. Phys. (in press).